IEEE Open Journal of Vehicular Technology

Received 30 March 2025; accepted 8 April 2025. Date of publication 14 April 2025;
date of current version 20 May 2025. The review of this article was coordinated by Editor Shuaishuai Guo.

Digital Object Identifier 10.1109/OJVT.2025.3560515

Performance Analyses of MRT/MRC in NOMA Full-Duplex Relay Networks With Residual Hardware Impairments

MESUT TOKA [1] (Member, IEEE), ERAY GÜVEN [2] (Graduate Student Member, IEEE), GÜNEŞ KARABULUT KURT [2] (Senior Member, IEEE), AND OĞUZ KUCUR [1] (Member, IEEE)

[1]Department of Electronics Engineering, Gebze Technical University, Gebze/Kocaeli 41400, Türkiye
[2]Poly-Grames Research Center, Department of Electrical Engineering, Polytechnique Montréal, Montréal, QC H3T 1J4, Canada

CORRESPONDING AUTHOR: GÜNEŞ KARABULUT KURT (e-mail: gunes.kurt@polymtl.ca).

This work was supported in part by the Scientific and Technological Research Council of Türkiye (TÜBİTAK) under Grant EEEAG 118E274 and in part by the Natural Sciences and Engineering Research Council of Canada (NSERC) Discovery Grant program.

ABSTRACT This paper analyzes the performance of maximum-ratio transmission (MRT)/maximum-ratio combining (MRC) scheme in a dual-hop non-orthogonal multiple access (NOMA) full-duplex (FD) relay networks in the presence of residual hardware impairments (RHIs). The effects of channel estimation errors (CEEs) and imperfect successive interference cancellation are also considered to deal with a more realistic scenario. In the network, the base station and multiple users utilize MRT and MRC, respectively, while a dedicated relay operates in amplify-and-forward mode. Exact outage probability (OP) expression is derived for Nakagami-*m* fading channels. Furthermore, tight lower bound and asymptotic expressions are also derived to provide further insights in terms of diversity order and array gain. The investigated network has been compared to half-duplex (HD)-NOMA and FD-orthogonal multiple access counterparts. The analytical results validated by simulations and test-bed implementations (by using software defined radios) demonstrate the importance of loop-interference cancellation process in the FD relay for the investigated system to perform better than HD-NOMA counterpart. Also, a performance trade-off between the MRT and MRC schemes is observed under CEE effects among users. Furthermore, it is shown that RHIs have a significant effect on the performance of users with lower power coefficients, however it does not change the diversity order. RHIs and CEEs have the most and least deterioration effects on the system performance, respectively.

INDEX TERMS Channel estimation error, full-duplex relay, imperfect successive interference cancellation, MIMO-NOMA, residual hardware impairments.

I. INTRODUCTION

For the last decade, many researchers from academia and industry have focused on non-orthogonal multiple access (NOMA) in order to overcome challenges caused by massively connected smart devices and fulfill requirements of forthcoming generation wireless networks, since the existing orthogonal multiple access (OMA) techniques are limited in terms of spectral efficiency and massive connectivity [1], [2]. The most important key feature of NOMA is to serve multiple users in the same resources (time/frequency/code) by allocating different power coefficients, and thus fairness among users can be ensured. Successive interference cancellation (SIC) technique is applied by users to separate the superposed signals and obtain the desired information related to user [3], [4]. So far, NOMA, especially power-domain NOMA, has been widely investigated in the literature in terms of fundamental aspects [5], [6], [7]. On the other hand, in order to exploit benefits of spatial diversity, multiple-input multiple-output (MIMO) techniques are also considered in NOMA networks [8], [9], [10], [11], [12], [13]. Also, exploiting machine learning and deep learning techniques is a focus of the literature to determine an appropriate solution for resource allocation and beamforming problems [14], [15].

Since relaying techniques offer extending coverage area and establish reliable communication under harsh channel environments and huge obstacles, recently, NOMA has been considered in cooperative and relaying transmission [16], [17]. The authors of [16] consider user-assisted relaying, while [17] investigates both user-assisted and dedicated relaying communication. In [18], outage probability (OP) analysis of a dual-hop amplify-and-forward (AF) relaying NOMA network, where the base station (BS) and users are equipped with single antenna each, has been conducted over Nakagami-m fading channels under channel estimation (CEE) effects. In [19], the authors have investigated transmit antenna selection (TAS) at the BS and maximal-ratio combining (MRC) at users in a dual-hop AF relaying NOMA system over Nakagami-m fading channels by considering CEEs. In [20], OP and ergodic capacity of cooperative two-user NOMA networks with direct link, where single relay among multiple relays and single antenna at users are selected, has been analyzed in the presence of CEEs and imperfect SIC (ipSIC). In [21], the authors have analyzed OP of a dual-hop MIMO-NOMA network, where maximal-ratio transmission (MRT)/receive antenna selection (RAS) are adopted in both hops, over Nakagami-m fading channels under CEE effects. However, studies mentioned above are based on half-duplex (HD) relaying technique. On the other hand, full-duplex (FD) relaying technique has emerged as a promising solution since the reception and transmission can be realized at the same time/frequency yielding double capacity. FD relay has a major drawback named loop interference (LI) caused by signal leakage between the transmitter and receiver antennas. Fortunately, thanks to the advances on antenna technologies and signal processing approaches, effect of LI can be reduced to a sufficient level in order for FD relaying be feasible in a practical manner [22]. Therefore, the authors of [23] and [24] have considered using FD relay in NOMA systems to overcome the loss of spectral efficiency caused by HD relays. Also, in [25], a cooperative two-user NOMA network based on cognitive radio is considered and joint beamforming optimization problem for transmit/receive ends at decode-and-forward (DF) FD relay is evaluated. The authors have also investigated MRT/zero-forcing (ZF), ZF/MRC and ZF/ZF schemes at the relay in a comparative manner. In [26], hybrid HD/FD relay-aided uplink NOMA network is considered in the presence of co-channel interference and ipSIC to investigate the deterioration in an uplink communication. The authors conducted performance evaluation over Rayleigh fading channels.

In practice, radio-frequency hardware components at the transmitter and receiver suffer from different impairments caused by high power amplifier non-linearity, in-phase/quadrature (I/Q) imbalance and phase noise, which seriously deteriorate the system performance due to mismatch between the desired and actual signal [27]. In order to compensate for the influence of these hardware impairments (HIs), a lot of efforts in developing appropriate approaches have been made in the literature; however, there still exist residual HIs (RHIs) which can not be overlooked in real-life deployments [28], [29]. Although some of the aforementioned studies on NOMA networks consider only CEEs, feedback delay (FBD), and ipSIC without RHIs in a practical manner; nevertheless, there are some works paying attention to effects of RHIs in NOMA networks. For instance, in [30], the impact of I/Q imbalance impairment in a secure single-input multiple-output (SIMO)-NOMA network consisting of one BS, multiple legitimate users and an eavesdropper has been investigated over Rayleigh fading channels. In order to utilize receive diversity, RAS scheme has been applied at receivers of all users and eavesdropper. In [31], outage performance of hybrid MRT/RAS scheme is investigated in single-hop multi-user NOMA system in the presence of RHIs together with CEEs and ipSIC. In [32], impact of RHIs on dual-hop multi-user NOMA network with AF relay has been investigated over Nakagami-m fading channels in terms of OP and ergodic rate. In [33], the authors analyzed OP and ergodic capacity of single-hop and dual-hop NOMA AF relay networks over $\alpha-\mu$ fading channels in the presence of CEEs, ipSIC and RHIs. In [34], a cooperative two-user NOMA network, where all nodes are equipped with single antenna and a DF hybrid HD/FD relay assists the communication between the BS and far user, has been investigated over Rayleigh fading channels in the presence of RHIs. To demonstrate the level of system performance, OP and ergodic capacity expressions have been obtained. In [35], the authors have considered the same system of [34] without direct link between the relay and near user, and analyzed OP and ergodic rate over Rician fading channels. In [36], the authors consider an overlay cognitive radio based on NOMA transmission using FD relay. They investigate the system in the presence of CEEs, ipSIC and RHIs, and propose a deep learning framework to predict ergodic sum-rate.

As seen above, there are many studies in the literature investigating effects of RHIs on single-hop and/or dual-hop NOMA networks with or without CEEs/ipSIC. However, the majority of them consider systems as consisting of HD relays and nodes equipped with single antenna except studies of [30], [34], [35], [36]. In [30], users and an eavesdropper are equipped with multiple antennas to adopt RAS scheme while FD relaying is considered in single antenna networks in [34], [35], [36]. Therefore, investigations on the impact of RHIs on both MIMO-NOMA and FD relaying based cooperative NOMA, to the best of our knowledge, are still limited. Motivated by [30], [34], [35], [36], in this paper, we investigate a dual-hop multi-user AF FD relaying based MIMO-NOMA system, where MRT and MRC schemes are exploited at the BS and users, respectively, over independent and identically distributed (i.i.d.) Nakagami-m fading channels in the presence of RHIs together with CEEs and ipSIC. Note that these three impairments together were not considered in dual-hop multi-antenna NOMA networks unlike dual-hop single antenna NOMA networks in [33], [36]. Contributions of the paper are summarized as follows:

- Unlike the existing studies on cooperative NOMA with RHIs, we consider using multiple antennas at the BS and users while the relay operates in FD mode. Furthermore,

our analyses have been conducted for a generic channel model, Nakagami-m fading, and LI link at the relay is also assumed to be exposed to fading variations.
- In order to deal with a more realistic scenario, CEEs and ipSIC have also been taken into account in the analyses. To characterize the system performance, exact OP expression for any user has been derived. Moreover, a tight lower bound and simple asymptotic expressions have been obtained to provide further insights, such as diversity behavior of the system. The investigated network has been compared to HD-NOMA and FD-OMA counterparts.
- Moreover, test-bed implementations by using USRP software defined radios (SDRs), which is the most sophisticated NOMA implementation in the literature, are conducted to demonstrate feasibility of the investigated system in a real-life manner.
- We have demonstrated that the quality of LI cancellation process is quite crucial for the investigated system to outperform HD-NOMA counterpart, even error floors may exist under the worst case of cancellation process. Performance improvement of MRT is much more than MRC in terms of users with lower power allocations in the absence of CEEs, while there is a trade-off between both schemes depending on the quality of channel conditions in the presence of CEEs. In addition, RHIs have much more effect on the performance of users with lower power allocations while do not change the diversity order of all users. Moreover, imperfections which have the most and least deterioration effects on the performance are RHIs and CEEs, respectively.

A. ORGANIZATION AND NOTATIONS

The rest of the paper is given as follows. In Section II, we introduce the system model and channel statistics including practical imperfections in detail. In Section III, we derive the exact OP expression for any user together with lower bound and asymptotic approximations. Section IV presents the test-bed implementations of the investigated system. Numerical results including comparisons are illustrated in Section V. Finally, conclusions are interpreted in Section VI.

Notation: Bold lowercase letter and $\|\cdot\|$ denote vectors and Euclidean norm while $(\cdot)^H$ indicates Hermitian transpose of a vector. $\mathbb{CN}(0,\sigma^2)$ is used to represent the complex Gaussian distribution with zero mean and variance of σ^2. While $Pr(\cdot)$ denote the probability of an event, $E[\cdot]$ represents the expectation operator. $f_X(\cdot)$ and $F_X(\cdot)$ indicate the probability density function (PDF) and cumulative distribution function (CDF) of a random variable X, respectively.

II. SYSTEM MODEL

We consider a dual-hop power domain downlink NOMA network, where one BS (S) communicates with L users (U_l, $l = 1,2,\ldots,L$) with assistance of an FD AF relay (R).[1] We assume that the direct link is not available due to huge obstacles and harsh environment conditions. The BS equipped with N_S antennas transmits information by applying MRT beamforming technique while users with N_D antennas combine received signals according to MRC scheme. Note that MRT and MRC schemes are the optimum ones among transmit and receive diversity techniques, respectively [37], [38]. On the other hand, the FD relay has two antennas, one for receiving and the other for broadcasting. $\mathbf{h}_{SR} = \{h_{SR}^i\}_{1\times N_S}$ $(1 \le i \le N_S)$, $\mathbf{h}_l = \{h_l^j\}_{N_D\times 1}$ $(1 \le j \le N_D)$ and h_{LI} denote channel coefficients corresponding to $S-R$, $R-U_l$ and $R-R$ links. Since channels are assumed to be distributed as i.i.d. Nakagami-m, squared of channel gains follow Gamma distribution, thus powers of links can be obtained by $\Omega_{SR} = E[|h_{SR}^i|^2] = d_{SR}^{-\alpha}$, $\Omega_l = E[|h_l^j|^2] = d_l^{-\alpha}$ and $\Omega_{LI} = E[|h_{LI}|^2] = \lambda P_R^{\mu-1}$, respectively. d_{SR} and d_l denote the normalized distances of $S-R$ and $R-U_l$ links, respectively, α is the path loss exponent. λ $(\lambda > 0)$ and μ $(0 \le \mu \le 1)$ represent the quality of LI cancellation process at $R-R$ link.[2]

Since effects of CEEs are also considered to be more practical, by following linear minimum mean square error estimation method, the BS and relay estimates channel coefficients in the training period, thus erroneously estimated channel coefficient vectors of $S-R$ and $R-U_l$ links can be represented by $\mathbf{h}_{SR} = \hat{\mathbf{h}}_{SR} + \boldsymbol{\varepsilon}_{e,SR}$ and $\mathbf{h}_l = \hat{\mathbf{h}}_l + \boldsymbol{\varepsilon}_{e,l}$, respectively.[3] $\boldsymbol{\varepsilon}_{e,SR}$ and $\boldsymbol{\varepsilon}_{e,l}$ are error vectors resulting from imperfect estimation process and can be modeled as $\boldsymbol{\varepsilon}_{e,SR} \sim \mathbb{CN}(0,\sigma_{e,SR}^2)$ and $\boldsymbol{\varepsilon}_{e,l} \sim \mathbb{CN}(0,\sigma_{e,l}^2)$ with variances of $\sigma_{e,SR}^2 = \Omega_{SR} - \hat{\Omega}_{SR}$ and $\sigma_{e,l}^2 = \Omega_l - \hat{\Omega}_l$, respectively [39].

Since the investigated system is based on NOMA transmission, the BS transmits superimposed signals represented by $x(n) = \sum_{i=1}^{L} \sqrt{P_S a_i} s_i(n)$ in the nth time interval, where P_S and a_i represent transmit power at the BS and power allocation coefficient intended to ith user ($\sum_{i=1}^{L} a_i = 1$), respectively. Note that we represented signals according to time index due to the FD relay transmission. Then, the received signal at the relay under RHIs effect can be represented as

$$y_R(n) = \mathbf{h}_{SR}(\mathbf{w}(n)x(n) + \boldsymbol{\eta}_{SR}(n)) + h_{LI}s_R(n) + n_R(n), \quad (1)$$

where $n_R(n) \sim \mathbb{CN}(0,\sigma_R^2)$ is Gaussian noise at R, and $\boldsymbol{\eta}_{SR}(n) = \{\eta_{SR}^i\}_{N_S\times 1}$ represents aggregate distortion noise (whose entries are subjected to $\mathbb{CN}(0,\kappa_{SR}^2 P_S)$) resulting from

[1] We consider AF protocol, because DF protocol necessitates digital-to-analog and analog-to-digital converters, and mixers, increasing hardware complexity and processing delay much more than AF.

[2] It is worthwhile noting that the FD relay suffers from a LI effect between transmit and receive antennas due to its inherent simultaneous transmission at the same time/frequency. Although LI effects have been mitigated somehow, there still remain some residual LI effects. Without loss of generality, we consider the residual LI model determined according to active and/or passive interference cancellation as in [22].

[3] Note that the utilized channel estimation model is widely considered in the existing literature [10], [21], [33].

RHIs at $S-R$ link. $\kappa_{SR}^2=(\kappa_S^t)^2+(\kappa_R^r)^2$ denotes aggregate power level of RHIs, where κ_S^t and κ_R^r are impairment levels [27], [28]. Since FD relay applies LI cancellation methods, we assume that the impact of RHIs distortion noise at link $R-R$ is absorbed by the LI cancellation parameter as in [40]. $\mathbf{w}(n)=\hat{\mathbf{h}}_{SR}^H/\|\hat{\mathbf{h}}_{SR}\|$ is MRT weight vector at the BS, subjected to $\|\mathbf{w}(n)\|^2=1$. Also, $s_R(n)=Gy_R(n-\tau)$ denotes the signal to be transmitted from the relay, where τ is processing delay of the FD transmission and G is the amplification factor which can be obtained as

$$G=\sqrt{\frac{P_R}{P_S(\|\hat{\mathbf{h}}_{SR}\|^2+\sigma_{e,SR}^2)(1+\kappa_{SR}^2)+P_R|h_{LI}|^2+\sigma_R^2}}. \quad (2)$$

Afterwards, the received signal vector at the lth user can be written as $\mathbf{y}_{U_l}(n)=\mathbf{h}_l(s_R(n)+\eta_{RU}(n))+\mathbf{n}_l(n)$, where $\mathbf{n}_l(n)=\{n_l^j(n)\}_{N_D\times 1}$ is Gaussian noise vector (whose entries are subjected to $\mathbb{CN}(0,\sigma_l^2)$) at lth user. Also, $\eta_{RU}(n)\sim\mathbb{CN}(0,\kappa_{RU}^2P_R)$ denotes the aggregate distortion noise of RHIs at $R-U_l$ link, where $\kappa_{RU}^2=(\kappa_R^t)^2+(\kappa_U^r)^2$ is aggregate power level of RHIs. Without loss of generality, as in [32], we consider that users have the same effect of hardware impairments; such that $\kappa_{U_l}^r\triangleq\kappa_U^r$. Then, if we substitute $s_R(n)$ into $\mathbf{y}_{U_l}(n)$, the received signal vector at lth user can be rewritten with the help of (1) as

$$\begin{aligned}\mathbf{y}_{U_l}(n)=\mathbf{h}_lG\mathbf{h}_{SR}\Bigg[&\underbrace{\mathbf{w}(n-\tau)\sqrt{P_Sa_l}s_l(n-\tau)}_{desiredsignal}\\&+\underbrace{\mathbf{w}(n-\tau)\sum_{p=1}^{l-1}\sqrt{P_Sa_p}s_p(n-\tau)}_{ipSICterm}\\&+\underbrace{\mathbf{w}(n-\tau)\sum_{k=l+1}^{L}\sqrt{P_Sa_k}s_k(n-\tau)}_{IUIterm}+\underbrace{\boldsymbol{\eta}_{SR}(n-\tau)}_{RHIsatS-R}\Bigg]\\&+\mathbf{h}_l\left[G\left(\underbrace{h_{LI}s_R(n-\tau)}_{LIterm}+n_R(n-\tau)\right)+\underbrace{\eta_{RU}(n)}_{RHIsatR-U_l}\right]\\&+\mathbf{n}_l(n). \quad (3)\end{aligned}$$

The received signals by N_D antennas at the lth user are combined according to MRC technique as $y_{U_l}^{MRC}=\mathbf{w}_{\mathrm{MRC}}(n)\mathbf{y}_{U_l}(n)$, where $\mathbf{w}_{\mathrm{MRC}}(n)=\hat{\mathbf{h}}_l^H/\|\hat{\mathbf{h}}_l\|$ is MRC weight vector subject to $\|\mathbf{w}_{\mathrm{MRC}}(n)\|^2=1$.

$$\gamma_{U_{j\to l}}=\frac{\psi_1\psi_2\bar{\gamma}^2a_j}{\psi_1\psi_2\bar{\gamma}^2(\xi_j+\tilde{\xi}_j+\vartheta_1)+\psi_1\bar{\gamma}\vartheta_2\vartheta_3+(\psi_2\bar{\gamma}+\vartheta_2)(\psi_3\bar{\gamma}\vartheta_4+\vartheta_5)\vartheta_3} \quad (4)$$

III. PERFORMANCE ANALYSES

In this section, end-to-end ($e2e$) signal-to-interference-distortion plus noise ratio (SIDNR) expression is derived. Then, the exact OP for any user is obtained together with lower bound and asymptotic expressions to provide further insights into the system performance.

A. DERIVATION OF e2e SIDNR

According to NOMA transmission, weaker users (with poorer channel qualities) are allocated higher power levels at the BS for ensuring the fairness. Therefore, in the training period, the relay estimates effective channel gains of $R-U_l$ links by using pilot symbols sent from all users such that they are ordered as $\|\hat{\mathbf{h}}_1\|^2\le\|\hat{\mathbf{h}}_2\|^2\cdots\le\|\hat{\mathbf{h}}_L\|^2$ without loss of generality, and then transmits the ordering to the BS and users at the same time. Thus, the BS allocates power coefficients to users as $a_1>a_2>\cdots>a_L$ by using the ordering. Also, the BS estimates channel gains of $S-R$ link to apply MRT beamforming. Since SIC is carried out at users, any stronger user l detects and removes signal of the weaker user j, where $j\le l$. On the other hand, signal of the stronger user k is considered as interference noise by user l, where $k>l$ and also named as inter-user interference (IUI). Consequently, by using (2) and (3), instantaneous SIDNR defined as the lth user detects the signal of jth user ($j\le l$) is given at the bottom of this page ($\gamma_{U_{j\to l}}$).

In (4), $\bar{\gamma}=P/\sigma^2$ represents average signal-to-noise ratio (SNR), where $P_S=P_R=P$ is assumed for mathematical simplicity, while $\xi_j=\sum_{k=j+1}^{L}a_k$ and $\tilde{\xi}_j=\sum_{p=1}^{j-1}a_p\sigma_{ipsic}^2$ are IUI and ipSIC terms, respectively. Without loss of generality, we assume that ipSIC is subject to Gaussian distribution with power σ_{ipsic}^2 ($0\le\sigma_{ipsic}^2\le 1$) as in [33], [41], [42]. Also, $\psi_1\triangleq\|\hat{\mathbf{h}}_{SR}\|^2$, $\psi_2\triangleq\|\hat{\mathbf{h}}_l\|^2$ and $\psi_3\triangleq|h_{LI}|^2$ definitions are made to simplify analyses. In addition, constant variables ϑ are given as: $\vartheta_1\triangleq\kappa_{SR}^2+\kappa_{RU}^2(1+\kappa_{SR}^2)$, $\vartheta_2\triangleq\bar{\gamma}\sigma_{e,l}^2+\frac{1}{1+\kappa_{RU}^2}$, $\vartheta_3\triangleq(1+\kappa_{RU}^2)(1+\kappa_{SR}^2)$, $\vartheta_4\triangleq\frac{1}{1+\kappa_{SR}^2}$, and $\vartheta_5\triangleq\bar{\gamma}\sigma_{e,SR}^2+\frac{1}{1+\kappa_{SR}^2}$.

B. OUTAGE PROBABILITY ANALYSIS

The outage event for the lth user can be defined as the lth user can not decode its own signal or the jth user's signal ($1\le j\le l$). Thus, let us define $E_{l,j}=\{\gamma_{U_{j\to l}}>\gamma_{th,j}\}$ as the event that the lth user can decode jth user's signal, where $\gamma_{th,j}=2^{R_0}-1$ (R_0: bits per channel in use (BPCU)) is the target threshold SIDNR for FD transmission. With the help of (4) and the event of $E_{l,j}$, the OP for the lth user can be written as

$$\begin{aligned}P_{out}^l&=1-Pr\left(E_{l,1}\cap E_{l,2}\cap\cdots\cap E_{l,l}\right)\\&=1-Pr\left(\psi_1>\frac{(\psi_2\bar{\gamma}+\vartheta_2)\times(\psi_3\bar{\gamma}\vartheta_4+\vartheta_5)\vartheta_3\delta_l^\dagger}{\bar{\gamma}(\psi_2-\vartheta_2\vartheta_3\delta_l^\dagger)},\psi_2>\vartheta_2\vartheta_3\delta_l^\dagger\right), \quad (5)\end{aligned}$$

which is subjected to the condition of $a_j-\gamma_{th,j}(\xi_j+\tilde{\xi}_j+\vartheta_1)>0$. Here, the notations $\delta_j\triangleq\frac{\gamma_{th,j}}{\bar{\gamma}(a_j-\gamma_{th,j}(\xi_j+\tilde{\xi}_j+\vartheta_1))}$ and

$\delta_l^\dagger = \max_{1\le j\le l}\{\delta_j\}$ are made for mathematical tractability. Note that, (5) holds for the condition of $a_j > \gamma_{th,j}(\xi_j + \tilde{\xi}_j + \vartheta_1)$, otherwise the OP results in 1. Then, (5) can be analytically expressed as

$$P_{out}^l = F_{\psi_2}^{(l)}(\vartheta_2\vartheta_3\delta_l^\dagger) + \int_{y=\vartheta_2\vartheta_3\delta_l^\dagger}^{\infty}\int_{z=0}^{\infty} F_{\psi_1}\left(\frac{(y\bar{\gamma}+\vartheta_2)(z\bar{\gamma}\vartheta_4+\vartheta_5)\vartheta_3\delta_l^\dagger}{\bar{\gamma}(y-\vartheta_2\vartheta_3\delta_l^\dagger)}\right) f_{\psi_3}(z) f_{\psi_2}^{(l)}(y)\,dz\,dy, \tag{6}$$

where $F_X^{(l)}$ and $f_X^{(l)}$ denote the CDF and PDF of user with the lth order statistic. Since channels are considered as i.i.d. Nakagami-m fading, it is well-known that the squared gain of any link will be distributed as Gamma. Thus, corresponding CDFs and PDF of random variables ψ_1, ψ_2 and ψ_3 can be represented as $F_{\psi_1}(x) = 1 - e^{-xm_{SR}/\hat{\Omega}_{SR}}\sum_{n=0}^{m_{SR}N_S-1}\frac{(xm_{SR}/\hat{\Omega}_{SR})^n}{n!}$, $F_{\psi_2}(x) = 1 - e^{-xm_l/\hat{\Omega}_l}\sum_{n_1=0}^{m_lN_D-1}\frac{(xm_l/\hat{\Omega}_l)^{n_1}}{n_1!}$ and $f_{\psi_3}(x) = (m_{LI}/\Omega_{LI})^{m_{LI}}\frac{x^{m_{LI}-1}}{\Gamma(m_{LI})}e^{-xm_{LI}/\Omega_{LI}}$. Here, m_{SR}, m_l, and m_{LI} denote Nakagami-m channel parameters related to $S-R$, $R-U_l$, and $R-R$ links, respectively. If $F_{\psi_1}(x)$ is substituted into (6) and then the integrals are rearranged, we obtain

$$P_{out}^l = 1 - \sum_{n=0}^{m_{SR}N_S-1}\frac{1}{n!}\int_{x=0}^{\infty} e^{-b} f_{\psi_2}^{(l)}(x+\vartheta_2\vartheta_3\delta_l^\dagger)dx \times \underbrace{\int_{z=0}^{\infty} e^{-za}(za+b)^n f_{\psi_3}(z)dz}_{I_1}, \tag{7}$$

where $a = \frac{(\bar{\gamma}(x+\vartheta_2\vartheta_3\delta_l^\dagger)+\vartheta_2)\vartheta_3\vartheta_4\delta_l^\dagger m_{SR}}{x\hat{\Omega}_{SR}}$ and $b = \frac{a\vartheta_5}{\bar{\gamma}\vartheta_4}$. By using binomial expansion [43, eq.(1.111)], integral property given by [43, eq.(3.381.4)] and $f_{\psi_3}(z)$, I_1 is obtained as

$$I_1 = \sum_{m=0}^{n}\binom{n}{m}\left(\frac{m_{LI}}{\Omega_{LI}}\right)^{m_{LI}}\frac{\Gamma(m+m_{LI})}{\Gamma(m_{LI})}\frac{b^{n-m}}{a^{-m}}\left(a+\frac{m_{LI}}{\Omega_{LI}}\right)^{-m-m_{LI}}, \tag{8}$$

where $\binom{\cdot}{\cdot}$ represents binomial coefficient, and thus (7) can be rewritten as

$$P_{out}^l = 1 - \sum_{n=0}^{m_{SR}N_S-1}\sum_{m=0}^{n}\binom{n}{m}\frac{(m_{LI}/\Omega_{LI})^{m_{LI}}}{\Gamma(m_{LI})}\frac{\Gamma(m+m_{LI})}{\Gamma(n+1)}\int_{x=0}^{\infty} e^{-b}\frac{b^{n-m}}{a^{-m}}\left(a+\frac{m_{LI}}{\Omega_{LI}}\right)^{-m-m_{LI}} f_{\psi_2}^{(l)}(x+\vartheta_2\vartheta_3\delta_l^\dagger)dx. \tag{9}$$

In order to proceed, $f_{\psi_2}^{(l)}(x)$ should be determined. By using order statistic properties [44], PDF of user with the lth order can be expressed as $f_{\psi_2}^{(l)}(x) = Q_l\sum_{s=0}^{L-l}\binom{L-l}{s}(-1)^s f_{\psi_2}(x)(F_{\psi_2}(x))^{l+s-l}$, where $Q_l = L!/((L-l)!(l-1)!)$ [5], [18]. If previously defined CDF of $F_{\psi_2}(x)$ and its derivative yielding PDF are substituted into $f_{\psi_2}^{(l)}(x)$, we get

$$f_{\psi_2}^{(l)}(x) = Q_l\sum_{s=0}^{L-l}\sum_{s_1=0}^{l+s-1}\sum_{n_1=0}^{s_1(m_lN_D-1)}\binom{L-l}{s}\binom{l+s-1}{s_1}(-1)^{s+s_1}\frac{(m_l/\hat{\Omega}_l)^{m_lN_D}}{\Gamma(m_lN_D)}\theta_{n_1}(s_1, m_lN_D)x^{n_1+m_lN_D-1}e^{-\frac{xm_l(s_1+1)}{\hat{\Omega}_l}}. \tag{10}$$

In order to obtain the closed-form of $f_{\psi_2}^{(l)}(x)$ in (10), binomial expansion [43, eq.(1.111)] and power series method given by [43, eq.(0.314)] are applied to $(F_{\psi_2}(x))^{l+s-l}$. Here, $\theta_{n_1}(s_1, m_lN_D)$ represents multinomial coefficient consisting of a recursive summation [10]. Finally, by substituting (10) into (9) and applying algebraic manipulations, the OP corresponding to the lth user can be obtained as given at the top of this page. In (11) shown at the bottom of the next page, $\Theta_l(x)$ can be expressed by

$$\Theta_l(x) = \int_{x=0}^{\infty} x^{n_2+n_3+m+m_{LI}-n} e^{-\frac{xm_l(s_1+1)}{\hat{\Omega}_l} - \frac{\left(\vartheta_2\vartheta_3\delta_l^\dagger+\vartheta_2/\bar{\gamma}\right)\vartheta_3\vartheta_5\delta_l^\dagger m_{SR}}{x\hat{\Omega}_{SR}}}\left(x+\frac{\vartheta_4(\bar{\gamma}\vartheta_2\vartheta_3\delta_l^\dagger+\vartheta_2)\vartheta_3\delta_l^\dagger m_{SR}\Omega_{LI}}{\bar{\gamma}\vartheta_3\vartheta_4\delta_l^\dagger m_{SR}\Omega_{LI}+m_{LI}\hat{\Omega}_{SR}}\right)^{-m-m_{LI}} dx. \tag{12}$$

As clearly seen in (11), it is difficult to infer considerable insights for the performance behavior due to the complicated form of the expression. Accordingly, we conduct lower bound and asymptotic analyses to gain further insights for the investigated system in the following subsections.

C. LOWER BOUND ANALYSIS

In order to find a tight approximation for the exact OP given by (11), SIDNR given in (4) can be upper-bounded, thus a tight lower-bound for the exact OP can be obtained. Firstly, (5) can be rewritten approximately as

$$P_{out}^l \approx 1 - Pr\left(\frac{W\frac{1}{\vartheta_4}\bar{\gamma}\psi_2\frac{1}{\vartheta_2}}{W\frac{1}{\vartheta_4}+\bar{\gamma}\psi_2\frac{1}{\vartheta_2}} > \bar{\gamma}\vartheta_3\delta_l^\dagger\right), \tag{13}$$

where $W = \bar{\gamma}\psi_1/(\bar{\gamma}\psi_3 + \vartheta_5/\vartheta_4)$ for mathematical simplicity. Then, by using the harmonic mean property of two random variables defined as $xy/(x+y) \le \min(x,y)$, lower-bound for the exact OP can be analytically expressed as

$$P_{out}^{l,low} = 1 - Pr\left(\min\left(W\frac{1}{\vartheta_4}, \bar{\gamma}\psi_2\frac{1}{\vartheta_2}\right) > \bar{\gamma}\vartheta_3\delta_l^\dagger\right) = 1 - \overline{F}_W\left(\bar{\gamma}\vartheta_3\vartheta_4\delta_l^\dagger\right)\overline{F}_{\psi_2}^{(l)}\left(\vartheta_2\vartheta_3\delta_l^\dagger\right). \tag{14}$$

In (14), the CDF of $F_W(x)$ can be mathematically expressed as

$$F_W(x) = Pr\left(\frac{\bar{\gamma}\psi_1}{\bar{\gamma}\psi_3 + (\vartheta_5/\vartheta_4)} \leq \underbrace{\bar{\gamma}\vartheta_3\vartheta_4\delta_l^{\dagger}}_{x}\right)$$
$$= 1 - \int_{y=0}^{\infty}\int_{x=x\left(y+\frac{\vartheta_5}{\bar{\gamma}\vartheta_4}\right)}^{\infty} f_{\psi_1}(x) f_{\psi_3}(y) dx dy. \quad (15)$$

Then, by substituting previously defined PDF of $f_{\psi_3}(x)$ and derivative of the CDF $F_{\psi_1}(x)$ into (15), we can obtain

$$F_W(x) = 1 - \sum_{n=0}^{m_{SR}N_S-1} \frac{1}{n!}\left(\frac{m_{LI}}{\Omega_{LI}}\right)^{m_{LI}} \frac{1}{\Gamma(m_{LI})}$$
$$\int_{y=0}^{\infty} y^{m_{LI}-1}\left(x\left(y+\frac{\vartheta_5}{\bar{\gamma}\vartheta_4}\right)\frac{m_{SR}}{\hat{\Omega}_{SR}}\right)^n$$
$$e^{-x\left(y+\frac{\vartheta_5}{\bar{\gamma}\vartheta_4}\right)\frac{m_{SR}}{\hat{\Omega}_{SR}} - y\frac{m_{LI}}{\Omega_{LI}}} dy. \quad (16)$$

With the help of integral property given by [43, eq.(3.381.4)], $F_W(x)$ can be derived as

$$F_W(x) = 1 - \sum_{n=0}^{m_{SR}N_S-1}\sum_{n_2=0}^{n}\binom{n}{n_2}\frac{(m_{LI}/\Omega_{LI})^{m_{LI}}}{\Gamma(m_{LI})}$$
$$\frac{(m_{SR}/\hat{\Omega}_{SR})^n}{\Gamma(n+1)}\Gamma(n_2+m_{LI})\left(\frac{\vartheta_5}{\bar{\gamma}\vartheta_4}\right)^{n-n_2}$$
$$x^n\left(\frac{x m_{SR}}{\hat{\Omega}_{SR}} + \frac{m_{LI}}{\Omega_{LI}}\right)^{-n_2-m_{LI}} e^{-\frac{x\vartheta_5 m_{SR}}{\bar{\gamma}\vartheta_4\hat{\Omega}_{SR}}}. \quad (17)$$

On the other hand, if the PDF of $f_{\psi_2}^{(l)}(x)$ given in (10) is integrated with respect to x, the CDF of $F_{\psi_2}^{(l)}(x)$ is obtained as

$$F_{\psi_2}^{(l)}(x) = 1 - Q_l\sum_{s=0}^{L-l}\sum_{s_1=1}^{l+s}\sum_{n_1=0}^{s_1(m_lN_D-1)}\binom{L-l}{s}$$
$$\binom{l+s}{s_1}\frac{(-1)^{s+s_1-1}}{l+s}\theta_{n_1}(s_1, m_lN_D)x^{n_1}e^{-\frac{x m_l s_1}{\hat{\Omega}_l}}. \quad (18)$$

If complementary versions of CDFs given in (17) and (18) are substituted into (14), a tight lower-bound of the exact OP corresponding to lth user can be obtained in closed-form.

D. ASYMPTOTIC ANALYSES

In order to reveal further insights for the system performance, asymptotic behavior of OP is considered by applying high SNR approximation in this subsection. Therefore, we have carried out the analyses according to two cases which are presented in the following subsections.

1) UNDER IDEAL CONDITIONS

• When the quality of LI cancellation is $\mu \neq 1$ (i.e., $0 < \mu < 1$) In the presence of ideal conditions (which means that there are no CEEs in the first and second hops), the system exploits benefits of diversity order and array gain at high SNR values (when $\bar{\gamma} \to \infty$). Thus, (13) can be approximated as

$$P_{out}^{l,\infty} \approx 1 - Pr\left(\frac{W\vartheta_1'\bar{\gamma}\psi_2\vartheta_2'}{W\vartheta_1' + \bar{\gamma}\psi_2\vartheta_2'} > \bar{\gamma}\vartheta_1'\vartheta_2'\delta_l^{\dagger}\right)$$
$$= 1 - Pr\left(\min\left(W\vartheta_1', \bar{\gamma}\psi_2\vartheta_2'\right) > \bar{\gamma}\vartheta_1'\vartheta_2'\delta_l^{\dagger}\right)$$
$$= F_W^{\infty}\left(\bar{\gamma}\vartheta_2'\delta_l^{\dagger}\right) + F_{\psi_2}^{(l),\infty}\left(\vartheta_1'\delta_l^{\dagger}\right), \quad (19)$$

where $W \simeq \psi_1/\psi_3$, $\vartheta_1' = 1 + \kappa_{SR}^2$ and $\vartheta_2' = 1 + \kappa_{RU}^2$ are defined. By using high SNR approximation approach [45], we can express asymptotic OP in (19) as in the form $P_{out}^{l,\infty} \approx (AG\bar{\gamma})^{-DO} + O(\bar{\gamma}^{-DO})$, where AG is the array gain, DO is the diversity order and $O(\cdot)$ represents high order terms to be neglected. Firstly, the asymptotic CDF of W can be derived by $F_W^{\infty}(x) = Pr(\psi_1/\psi_3 \leq x) = \int_{y=0}^{\infty} F_{\psi_1}^{\infty}(yx) f_{\psi_3}(y) dy$. Here, the CDF of ψ_1 is expressed as $F_{\psi_1}(x) = \frac{\gamma(m_{SR}N_S, x m_{SR}/\Omega_{SR})}{\Gamma(m_{SR}N_S)}$ in terms of lower incomplete Gamma function [43, eq.(8.350.1)], then it can be asymptotically obtained as $F_{\psi_1}^{\infty}(x) \approx \frac{(x m_{SR}/\Omega_{SR})^{m_{SR}N_S}}{\Gamma(m_{SR}N_S+1)}$ by using the property of $\gamma(x, y \to 0) \approx y^x/x$ [46, eq.(45:9:1)]. If $F_{\psi_1}^{\infty}(x)$ and previously defined $f_{\psi_3}(y)$ are substituted into $F_W^{\infty}(x)$ by replacing x with $\bar{\gamma}\vartheta_2'\delta_l^{\dagger}$, we obtain $F_W^{\infty}(\bar{\gamma}\vartheta_2'\delta_l^{\dagger}) = (\chi_1\bar{\gamma})^{-(1-\mu)m_{SR}N_S}$, where χ_1 can be obtained as

$$P_{out}^{l} = 1 - Q_l\sum_{n=0}^{m_{SR}N_S-1}\sum_{m=0}^{n}\sum_{s=0}^{L-l}\sum_{s_1=0}^{l+s-1}\sum_{n_1=0}^{s_1(m_lN_D-1)}\sum_{n_2=0}^{n_1+m_lN_D-1}\sum_{n_3=0}^{n}\binom{n}{m}\binom{L-l}{s}\binom{l+s-1}{s_1}\binom{n_1+m_lN_D-1}{n_2}\binom{n}{n_3}$$
$$(-1)^{s+s_1}\frac{\Gamma(m+m_{LI})(m_{LI}/\Omega_{LI})^{m_{LI}}(m_l/\hat{\Omega}_l)^{m_lN_D}}{\Gamma(n+1)\Gamma(m_{LI})\Gamma(m_lN_D)}\theta_{n_1}(s_1, m_lN_D)(\vartheta_2\vartheta_3\delta_l^{\dagger})^{n_1+m_lN_D-n_2-1}e^{-\frac{(\vartheta_2\vartheta_3\delta_l^{\dagger})m_l(s_1+1)}{\hat{\Omega}_l} - \frac{\vartheta_3\vartheta_5\delta_l^{\dagger}m_{SR}}{\hat{\Omega}_{SR}}}$$
$$\left(\frac{\bar{\gamma}\vartheta_4}{\vartheta_5}\right)^m\left(\frac{\vartheta_3\vartheta_5\delta_l^{\dagger}m_{SR}}{\hat{\Omega}_{SR}}\right)^n\left(\vartheta_2\vartheta_3\delta_l^{\dagger} + \frac{\vartheta_2}{\bar{\gamma}}\right)^{n-n_3}\left(\Omega_{LI}\hat{\Omega}_{SR}\right)^{m+m_{LI}}\left(\bar{\gamma}\vartheta_3\vartheta_4\delta_l^{\dagger}m_{SR}\Omega_{LI} + m_{LI}\hat{\Omega}_{SR}\right)^{-m-m_{LI}}\Theta_l(x). \quad (11)$$

$$\chi_1 = \left(\frac{\Gamma(m_{SR}N_S + m_{LI})}{\Gamma(m_{SR}N_S + 1)\Gamma(m_{LI})} \left(\frac{\vartheta_2' \Lambda_l^\dagger m_{SR}}{\Omega_{SR} m_{LI}} \right)^{m_{SR}N_S} \right)^{-\frac{1}{(1-\mu)m_{SR}N_S}}. \tag{20}$$

In (20), $\Lambda_l^\dagger = \bar{\gamma}\delta_l^\dagger$ and independent from $\bar{\gamma}$. Therefore, the exponentially dominant constant on the average SNR ($\bar{\gamma}$) within the expression of $F_W^\infty(\bar{\gamma}\vartheta_2'\delta_l^\dagger)$ equals to $(1-\mu)m_{SR}N_S$ for the first hop. Asymptotic expression of $F_{\psi_2}^{(l),\infty}(x)$ can be derived by taking into account of lower order terms related to variable of x in (18) as $F_{\psi_2}^{(l),\infty}(x) \approx \binom{L}{l}(\frac{(x m_l/\Omega_l)^{m_l N_D}}{\Gamma(m_l N_D+1)})^l$. Afterwards, by replacing x with $\vartheta_1'\delta_l^\dagger$ and after mathematical manipulations, we obtain $F_{\psi_2}^{(l),\infty}(\vartheta_1'\delta_l^\dagger) = (\chi_2\bar{\gamma})^{-m_l N_D l}$, where χ_2 can be found as

$$\chi_2 = \left(\binom{L}{l} \frac{1}{(\Gamma(m_l N_D + 1))^l} \right)^{-\frac{1}{m_l N_D l}} \frac{\Omega_l}{\vartheta_1' \Lambda_l^\dagger m_l}. \tag{21}$$

From (21), the exponentially dominant constant on the average SNR ($\bar{\gamma}$) within the expression of $F_{\psi_2}^{(l),\infty}(\vartheta_1'\delta_l^\dagger)$ equals to $m_l N_D l$ for the second hop. Consequently, if $F_W^\infty(\bar{\gamma}\vartheta_2'\delta_l^\dagger)$ and $F_{\psi_2}^{(l),\infty}(\vartheta_1'\delta_l^\dagger)$ are substituted into (19), and with the help of asymptotic form $P_{out}^{l,\infty} \approx (AG\bar{\gamma})^{-DO} + O(\bar{\gamma}^{-DO})$, the asymptotic OP of the lth user can be obtained in simple form with diversity order metric $DO = \min\{(1-\mu)m_{SR}N_S, m_l N_D l\}$. Further, array gain can be found by using (20) and (21) as

$$AG = \begin{cases} \chi_1 & (1-\mu)m_{SR}N_S < m_l N_D l \\ \chi_2 & (1-\mu)m_{SR}N_S > m_l N_D l \\ \chi_1 + \chi_2 & (1-\mu)m_{SR}N_S = m_l N_D l \end{cases}. \tag{22}$$

• When the quality of LI cancellation is $\mu = 1$

In this case, $S-R$ link will be extremely dominant in *e2e* SIDNR due to the high LI effect. Therefore, asymptotic OP for the lth user can be expressed as $P_{out}^{l,\infty} \approx F_W(\vartheta_2'\Lambda_l^\dagger)$, where $W \approx \psi_1/\psi_3$, by neglecting the effect of $R-U_l$ link for high SNR values. Since $F_W(\vartheta_2'\Lambda_l^\dagger)$ is independent from average SNR which also yields error floor level at high SNR values (also means zero diversity), we can not carry out high SNR approximation provided in [45]. Therefore, $F_W(x)$ can be obtained as

$$F_W(x) = Pr\left(\frac{\psi_1}{\psi_3} \leq \underbrace{\vartheta_2'\Lambda_l^\dagger}_{x} \right) = 1 - \int_{y=0}^{\infty} \int_{x=xy}^{\infty} f_{\psi_1}(x) f_{\psi_3}(y) dx dy. \tag{23}$$

Then, by substituting the PDF of ψ_1 to get rid of the inner integral and the PDF of ψ_3 into (23), and with the help of integral property provided by [43, eq.(3.381.4)], the asymptotic OP of the lth user can be derived as

$$P_{out}^{l,\infty} = 1 - \sum_{n=0}^{m_{SR}N_S-1} \frac{(m_{LI}/\Omega_{LI})^{m_{LI}} (m_{SR}/\Omega_{SR})^n}{\Gamma(n+1)\Gamma(m_{LI})} \Gamma(n+m_{LI})(\vartheta_2'\Lambda_l^\dagger)^n \left(\frac{\vartheta_2'\Lambda_l^\dagger m_{SR}}{\Omega_{SR}} + \frac{m_{LI}}{\Omega_{LI}} \right)^{-n-m_{LI}} \tag{24}$$

As seen in (24), the OP is not dependent on average SNR ($\bar{\gamma}$).

2) UNDER PRACTICAL CONDITIONS

Since CEE parameters $\sigma_{e,l}^2$ and $\sigma_{e,SR}^2$ are dominant on the *e2e* SIDNR, we can not apply asymptotic property $\gamma(x, y \to 0) \approx y^x/x$ given in [46, eq.(45:9:1)]. Thus, by considering the dominance of CEE effects, in case of all quality of LI cancellation values (μ), the predefined constants of ϑ_2 and ϑ_5 can be approximated as $\vartheta_2 \approx \bar{\gamma}\sigma_{e,l}^2$ and $\vartheta_5 \approx \bar{\gamma}\sigma_{e,SR}^2$, respectively. By substituting ϑ_2 and ϑ_5 together with other ϑ constants into (11), asymptotic OP of lth user in the presence of CEEs can be obtained.

Remark 1: Overall, the following inferences can be made with the asymptotic analyses performed above. On the one hand, in the presence of CEEs in both hops, the system cannot take advantage of diversity order and array gain regardless of whether LI cancellation process is perfect or not. On the other hand, under ideal conditions (that is, no CEEs in both hops), we should investigate the OP behavior in two cases to infer more insights. For the first case, where the quality of LI cancellation is at a good level ($\mu \neq 1$), the system enjoys the benefits of diversity order and array gain, that is, $DO = \min\{(1-\mu)m_{SR}N_S, m_l N_D l\}$. One can see that the quality of LI cancellation (with the parameter μ) has an effect in the first hop of the network. If the diversity order is $DO = (1-\mu)m_{SR}N_S$, RHI in the second hop has the most effect on the system performance. As the quality of LI cancellation increases, the adverse effect of RHI decreases. If the diversity order is limited by the second hop ($DO = m_l N_D l$), RHI in the first hop has the most effect on the system performance. Also, the quality of LI cancellation does not have an impact.

IV. TEST-BED IMPLEMENTATION

A real-time practical test for the investigated dual-hop FD-NOMA with MRT/MRC system was conducted by using SDRs to support the theoretical analysis.[4] In order to observe the performance of the MRT/MRC scheme, antenna configuration has been set as ($N_S = 2; N_D = 2$). Apart from this main test, a trial test was run in order to validate the determined system parameters and channel model, as will be explained later on. The trial test includes neither the disruptive panel nor the distance variations, unlike the main test; therefore it is only the supportive experiment to find out related parameters to be used for the main test.

[4]Test-bed implementation was realized at Istanbul Technical University Wireless Communications Research Laboratory, Istanbul, Turkey.

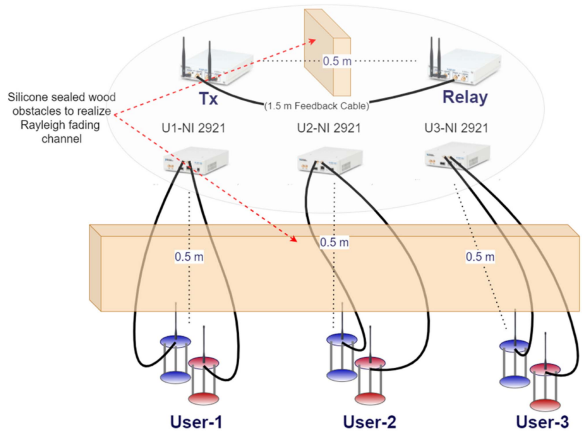

FIGURE 1. Test-bed set-up for dual-hop FD-NOMA with MRT/MRC system.

For the considered downlink scenario, one USRP-2901 transmitter acting as the BS, a USRP-2921 operating as the FD relay, and 3 USRP-2921 as the receivers were used to establish the test-bed set-up as given in Fig. 1 (next page). While both models of radios can run in FD mode, the main difference between the USRP-2921 and the USRP-2901 is that the USRP-2921 has a higher sample-per-second rate than the USRP-2901 model. During the experiment, SDRs were configured for the same data transfer rates.

A total of 3 separate algorithms (BS, Relay, and User) were conducted over the LabVIEW program and run by two separate host computers. The test was taken by tuning the transmitter gain to match different SNR values. Note that the signal received by the relay has been transmitted as it is, without being neither resampled nor decoded. The trial test examined disruptive factors such as signal interference and LI cancellation parameters, as will be discussed later. While the computer with an Intel-Xeon E5-1620 processor managed the relay operations, a personal host computer controlled BS, users, and receiver-relay operations. In our system, a CDA-2990 model ± 20 μ s precision with oven-controlled crystal oscillators is used for synchronization between transmitter and receiver, which can provide a high-resolution reference 10 MHz signal with 25 ppb frequency accuracy. In the test conducted indoor, all antennas were identical, omnidirectional, and had 3 dBi gain. User antennas were placed at the same distances from the relay to diversify users' channel difficulties, using 1.5 m long coaxial cables. In this test, distances are set as $d_{SR} = d_1 = d_2 = d_3 = 0.5$ m. Without loss of generality, we assume that the first user (U_1) is the weakest user with the lowest channel gain while the third user (U_3) is the strongest one with the highest channel gain. Another detail regarding the test environment is to prevent line-of-sight and create a Nakagami-m distributed fading channel with parameter $m = 1$ (in other words Rayleigh channel) by placing 1 m $\times$ 4 m sized silicon-coated wood panel sheets between each hop.

A. EXPERIMENTS

1) ACQUIRING THE PARAMETERS

In order to evaluate the impact of different parametric conditions on each NOMA user, we found it appropriate to maintain a consistent user index, initially determined based solely on effective channel gains. Before starting the test measurements, firstly, power coefficient a_1 was allocated to the weakest user with the lowest estimated effective channel gain value, a_3 was allocated to the strongest user with the highest estimated effective channel gain value, and a_2 was allocated to the middle user (U_2). In order to minimize the interference between users in real-time experiments and ensure the user fairness, the power coefficients were determined as $a_1 = 1/2$, $a_2 = 1/3$ and $a_3 = 1/6$. The threshold SINR values for the outage are determined as $\gamma_{th,1} = 0.9$, $\gamma_{th,2} = 1.5$, and $\gamma_{th,3} = 2$. These values remain constant throughout the test. After the power determination for the users, to characterize the shape factor of the Nakagami-m fading, the channel coefficients have been estimated by using single-input single output (SISO) and single carrier-OMA data transfer between BS-Relay and approximated by the maximum likelihood estimation, consequently we found it as approximately $m = 1.33$. In addition, the mean square error amounts of the channel estimations were recorded in a noise-free simulation environment by using the transmitted and received pilot symbols at the end. As a crucial point regarding CEE, the whole system contains CEEs that cannot be ignored during the channel state information (CSI) transmission between the relay and BS. Note that it is not possible to estimate the RHI effect in whole system by using the hardware itself, thus RHIs parameters (κ_{SR} and κ_{RU}) are quite unknown and unpredictable in this study. In addition, SIC processes at the receivers are also imperfect. The CSI required for the MRT operation of the test is found by decoding the single-carrier signal sent from the relay operating in AF mode, so that the instantaneous CSI between the BS and relay is constantly available in the BS. The experiment consists of taking the instantaneous SNR values after MRC processes and performing outage calculation for transmitted data packets performed at different transmitter SDR gains. The SNR value for test points taken in discrete time is shown to be equal to the mean of the total SNR values received in the set. As mentioned before, while the gains of the receiver and relay radios were kept constant in the test, the output power of the BS was changed to reach different SNR regions. The operating frequency for the test was chosen as 2.11 GHz. The bandwidth used for 500,000 samples transferred per second corresponds to 400 kHz for these particular USRPs.

B. TEST CONFIGURATION

Test measurement steps for dual-hop FD-NOMA with MRT/MRC system are as follows. 128-bit strings belonging to all users at the BS are multiplied by the power coefficients assigned to them right after they are modulated by BPSK and added together to form a single 128-bit signal, namely the superimposed NOMA signal. This signal is preceded by a 48-bit barker string for synchronization. Then, a total of 17 pilots are added to predict the channel information, with 1 pilot symbol coming after every 8 information symbols. After 8-factor sampling process is done, samples are sent to the relay through the matched filter convolution. Containing

1,544 samples per cycle, the test stops single set measurement process after a total of 10,000 cycles.

After adding the pilot and barker, the MRT diversity technique is applied to the BS. In addition to the relay's AF operation, the same relay also provides data flow to the BS, allowing the BS to have CSI by estimating the channel just like all users do. As explained, the BS no longer only transmits data but also obtains the channel information of the link BS-R over a wired connection from the relay itself, and it uses this information for the diversity operation. A 1.5 m coaxial cable is used to make this one way connection to minimize any disruptive effects in the feedback channel. While the estimated channel is $h = |h|e^{j\theta}$, the data to be transmitted is converted into $x' = [x_1 \;\; x_2][e^{-j\theta_1} \;\; e^{-j\theta_2}]^T$ in a precoding approach. Thus, the MRT beamforming process is completed, and the test continues with the sampling and transmission to the relay.

The first hop relay operation is done by buffering the complex data that was received by the relay SDR during the test. The second hop process is completed by transferring the buffered data to the users by amplifying the signal with 42 dB transmitter gain. After the incoming signals of the users' antennas with different channels on the user radio are resampled, the decoding process is started. It should be noted that users fully have the knowledge of both true pilot and preamble symbols. Synchronization processes occur when repetitive preamble sequences added per symbol at the source are detected at the point at which autocorrelation reaches its maximum at the receiver input. After this error is compensated, the estimation of the carrier frequency offset (CFO) arising from both the hardware and the channel exposure are found practically by averaging the phase differences of the sequential barker symbols and corrected with the inverse of the estimated phase. After these processes, the effect of the merged dual-hop channel is estimated by using the LS-based linear estimation method by means of the pilots interleaved into the data. The received signal matrix is $\mathbf{y} = [y_1 \;\; y_2]^T$ and the estimated channel is $\mathbf{h}_e = [h_{e_1} \;\; h_{e_2}]$ where h_{e_1} belongs to the first antenna and h_{e_2} belongs to the second antenna. The equalized signal according to the MRC technique equals to $\bar{x} = \mathbf{h}_e^H \mathbf{y} / \|\mathbf{h}_e\|^2$. Thus, by using one estimated channel vector and one non-equalized data for each antenna, the MRC process is applied, and the signal equalization process is completed. For user detection, the SIC algorithm is applied as in [47], while each user obtains its own data, other users are assumed as noise for the first user, and this user is exempt of SIC. Thus, the users get their own bits by going through the demodulation operation.

The pilots used for channel estimation are also used for SNR estimation. The SNR value was obtained by using the error vector magnitude (EVM) values of these pilots [48]. Since this measurement, which was calculated as the SNR value, also included the imperfect SIC and IUI effects, this value was accepted as SIDNR. This estimation error was found by the same linear minimum mean square error (LMMSE) method used in the theoretical analysis by running the simulation of the noise-free test system. The variance of CEE found as $\sigma^2_{cee} = 0.0388$ for a single hop, and it is assumed to be equal for both $\sigma^2_{e,l}$ and $\sigma^2_{e,SR}$, since no decoding operation is performed at the relay. Note that since the channel gain found by trial test containing all pilot data cannot indicate the channel with 100%, the practically found CEE also contains errors. In the last step, test is completed by performing an outage calculation with the threshold values for the previously determined system.

C. IMPLEMENTATION REMARKS

The main issues and points worth to be emphasized during real-time testing are as follows:

- Considering that it is not possible to observe the perfect SIC in the test environment, the imperfection at users with SIC was estimated as the variance of channel gains relative to the first user without SIC. To quantify non-ideal conditions, signals were normalized with their power coefficients so that the only difference between users was SIC. According to mean square error of the U_2 to U_1, σ^2_{ipsic} equals to 0.028.
- In the total of 10,000 packet transfers for each user, every fifth packet had to be skipped due to the memory limitations of the host devices during the data buffering. Due to the independence of the packages from each other, it has no effect on the test in terms of performance regarding these uncovered data whatsoever. In summary, each user kept and processed 8,000 of the 10,000 packages and ignored 2,000.
- Performance analysis of each user is done one by one for the sake of simplicity. Thereby, IUI can be neglected. Considering that there is no uplink, it is reasonable to assume that it does not cause an impact on test results.
- For the artificial Nakagami-m distributed environment made by using panels, a one-time channel distribution measurement containing 4.6 million channel coefficients has been done. This measurement was made by single carrier transmission and using the same least square estimation (LSE) channel estimation method used in the tests with OMA structure. The distribution of the absolute values of the channel coefficients was obtained and the shape factor of this distribution was measured as $m = 1.33$ by the maximum likelihood estimation for Nakagami-m distribution. This result for one hop was used for both hops in the simulations.
- Compared to theoretical analysis, in practical applications, the SIDNR value cannot be known and can only be estimated [49]. While it is impossible to attain i.i.d. white noise alone, in addition, the instantaneous strength of interference caused by another signal is also a question mark. While measuring the SNR value with the help of the pilot used in the tests, CEE was also practically exposed. Although the pilot powers are increased to minimize this error, it is not possible to completely eliminate the error.

- Throughout the test, some of the external factors that have been observed to affect the measurements are as follows: attenuation caused by the coaxial cable, reflections of the objects in the test environment, ambient temperature and humidity, and noise figure between $5-7$ dB of the equipment. The measurements were taken without using any shielding and screening methods, and it is known that they are exposed to crosstalk and EMI effects between devices. In a study examining the size of this distortion belonging to USRP model radios [50], it has been observed that it has a crosstalk power of about -50 dB. In addition, the tests were carried out without limiting the frequency operation ranges and maximum bandwidths of the radios, and it is thought that the synchronization module, which makes the devices independent from the internal timing and frequency structure, eliminates the impairments of the tests to a great extent.
- LI cancellation parameters of FD operation were also measured in the trial run. After examining the relative variability of λ and μ in the test system, this relation was used in the simulations. While P_{in} reaching the relay equals to 0.0045 W, P_R becomes 0.09 W with 20 dB relay receiver gain ($\Omega_{LI} = E[|h_{LI}|^2] = \lambda P_R^{\mu-1}$).
- The mismatch in the high-SNR region between theoretical predictions and testbed results is due to aggregated RHI when the USRP gain is constrained by the non-linearity of the built-in amplifier (e.g., third-order intercept point). To mitigate this, high gain on SDRs is avoided.
- Due to non-line of sight (NLOS) paths, users experience varying channel gains from multipath components. While strong fading is undesirable, it enhances SIC by introducing channel diversity [51].

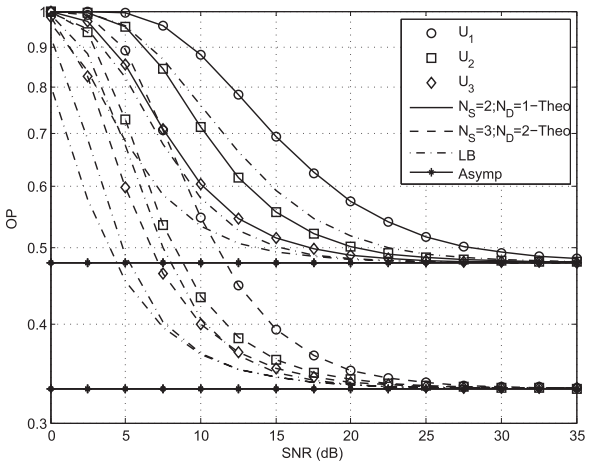

FIGURE 2. OP of the investigated system in case of $\mu = 1$ and ideal conditions.

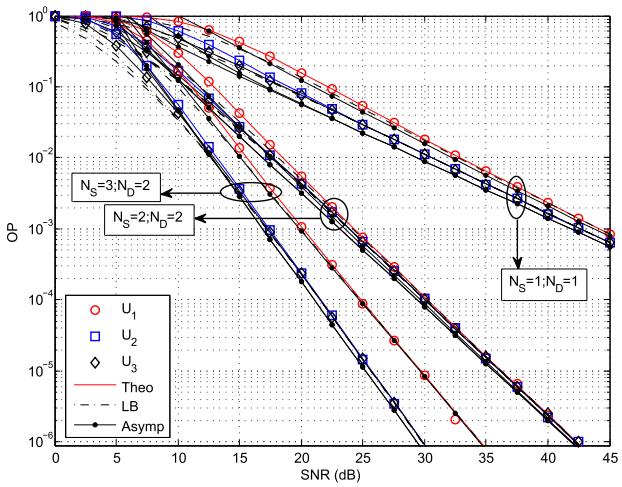

FIGURE 3. OP of the system in case of different antenna configurations under ideal conditions.

V. NUMERICAL RESULTS

In this section, theoretical results for the investigated system verified by Monte Carlo simulations are presented. An exemplary, the scenario with three mobile users ($L = 3$) is considered. Unless otherwise stated, markers illustrate simulation results, SNR $= \bar{\gamma} = P/\sigma^2$, $\alpha = 3$ (for urban area cellular radio), $\lambda = 1$ as in [22]. While power coefficients to be allocated to users are set as $a_1 = 1/2$, $a_2 = 1/3$ and $a_3 = 1/6$, target SIDNR thresholds related to mobile users for FD transmission are determined as $\gamma_{th,1} = 0.9$, $\gamma_{th,2} = 1.5$ and $\gamma_{th,3} = 2$, respectively. Also, normalized distances of $S-R$ link and $R-U_l$ links are fixed as $d_{SR} = 0.5$ and $d_1 = d_2 = d_3 = 0.5$, respectively. For simplicity, Nakagami-m channel parameters of $R-U_l$ links are assumed as $m_1 = m_2 = m_3 = m_{RU}$. For ease of reading, lower bound (LB), asymptotic (Asymp) and theoretical (Theo) abbreviations are made.

Fig. 2 depicts OP curves of the investigated system in case of $\mu = 1$ (which means the worst scenario of LI cancellation process), $m_{SR} = m_{LI} = m_{RU} = 1$, $\sigma^2_{ipsic} = 0$, $\kappa_{SR} = \kappa_{RU} = 0$ under ideal channel conditions ($\sigma^2_{e,SR} = 0$ and $\sigma^2_{e,l} = 0$) for different antenna configurations. We observe from the figure that OP performance of the investigated system is strictly limited by error floor level, which is also known as zero-diversity and validated by asymptotic results, at high SNR values for all users. Also, OPs of all users are exposed to the same level regardless of the number of antennas. On the other hand, given the increased number of antennas (when the configurations $N_S = 3$; $N_D = 2$ and $N_S = 2$; $N_D = 1$ are compared), performance of the system can be improved in the low SNR region and with the decrease of error floor level in the high SNR region. In addition, we also observed that the exact results are supported by LB curves which are quite tight and match well in the high SNR region.

Fig. 3 illustrates OP performance of the system for different antenna configurations for $\mu = 0.2$, $m_{SR} = m_{LI} = m_{RU} = 1$, $\sigma^2_{e,SR} = \sigma^2_{e,l} = 0$, $\sigma^2_{ipsic} = 0$ and $\kappa_{SR} = \kappa_{RU} = 0$. As clearly

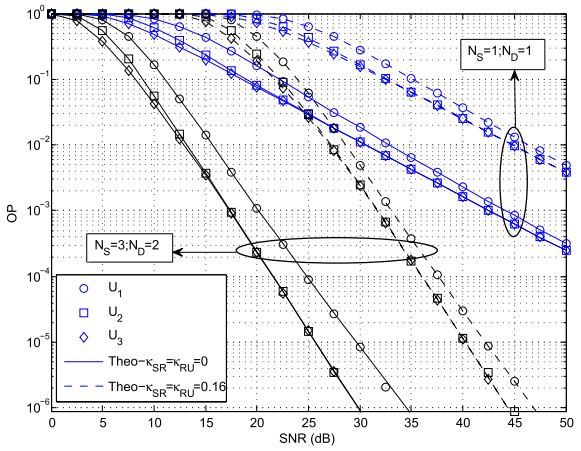

FIGURE 4. OP of the system in case of different antenna configurations and RHIs.

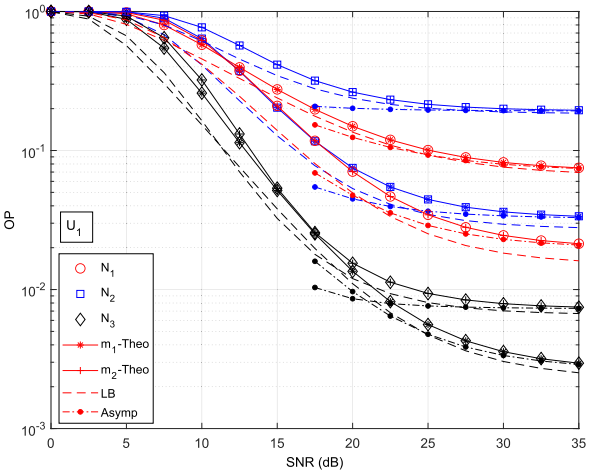

FIGURE 5. OP of the first user in case of $\mu = 0.2$, different fading and antenna configurations under CEEs.

observed from the figure, there is no error floor level when $\mu \neq 1$, and thus all users enjoy benefits of diversity order in the high SNR region. This result is also verified by the asymptotic curves which are obtained by theoretical analyses. Particularly, according to results of the first user, diversity orders are $(1-\mu)m_{SR}N_S$ for $N_S = 1$; $N_D = 1$ and $N_S = 2$; $N_D = 2$ configurations, and $m_{RU}N_D l$ for $N_S = 3$; $N_D = 2$ configuration, respectively. Also, if $N_S = 3$; $N_D = 2$ and $N_S = 2$; $N_D = 2$ configurations are compared for OP= 10^{-5}, 11 dB more SNR gain can be achieved for the second and third users while 7 dB for the first user, which implies that MRT beamforming is much more effective on the performance of the second and third users than first user.

In Fig. 4, OP performance of the system is presented for different RHIs parameters and antenna configurations. All curves are obtained for $\mu = 0.2$, $\sigma^2_{e,SR} = \sigma^2_{e,l} = 0$, $\sigma^2_{ipsic} = 0$ and $m_{SR} = m_{LI} = m_{RU} = 1$. From the figure, we observed that RHIs highly deteriorate the performance of users if $\kappa_{SR} = \kappa_{RU} = 0$ and $\kappa_{SR} = \kappa_{RU} = 0.16$ configurations are compared. Particularly, according to $N_S = 3$; $N_D = 2$ results, performance gap between $\kappa_{SR} = \kappa_{RU} = 0$ and $\kappa_{SR} = \kappa_{RU} = 0.16$ in terms of the second and third users is approximately 15 dB for an OP value of 10^{-5} while 12.5 dB in terms of the first user. Similar results are obtained for $N_S = 1; N_D = 1$ configuration. This result reveals that the impact of RHIs is more effective on the performance of the second and third users relative to the first user. A significant performance gain can be achieved as the number of antennas is increased, even under the effect of RHIs. Moreover, diversity order of the system is not affected by RHIs and asymptotic analysis also validates this observation.

Figs. 5 and 6 depict OP curves of three users in the presence of practical channel conditions ($\sigma^2_{e,SR} = \sigma^2_{e,l} = 0.03$) for $\mu = 0.2$, $\sigma^2_{ipsic} = 0$ and $\kappa_{SR} = \kappa_{RU} = 0$. In both figures, antenna configurations are set as N_1:($N_S = 1; N_D = 2$), N_2:($N_S = 2; N_D = 1$) and N_3:($N_S = 2; N_D = 2$) while channel parameters are m_1:($m_{SR} = 1; m_{LI} = 1; m_{RU} = 2$) and m_2:($m_{SR} = 2; m_{LI} = 1; m_{RU} = 1$). In both figures, we observe error floor levels in the high SNR region caused by the effects of CEEs, even $\mu \neq 1$. From Fig. 5, if we compare N_1 (also means MRC) and N_2 (also means MRT) configurations, MRT is better than MRC when the channel condition in the second hop is better (m_1 conf.), while MRC is better than MRT when the channel condition in the first hop is better (m_2 conf.). Consequently, performance behavior of the first user according to MRT and MRC schemes also depend on the channel conditions. Also, similar observations are obtained for the second and third users from Fig. 6. Furthermore, as clearly seen in both figures, although MRT and MRC schemes improve the performance of the system, hybrid scheme of MRT/MRC significantly increases OP performance of all users. Note also that hybrid scheme performs better in the low SNR region, significantly better in the high SNR region for m_1 configuration.

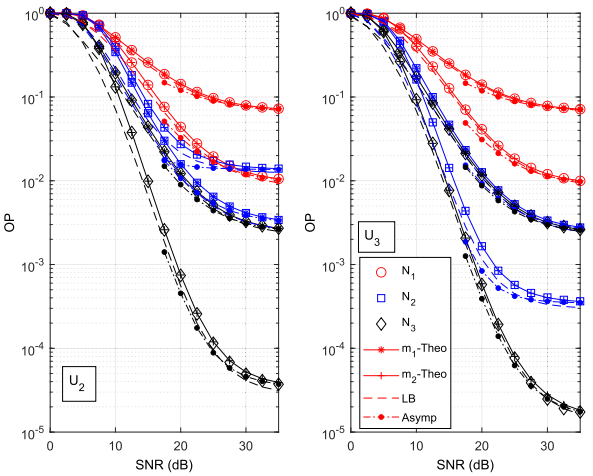

FIGURE 6. OP of the second and third users in case of $\mu = 0.2$, different fading and antenna configurations under CEEs.

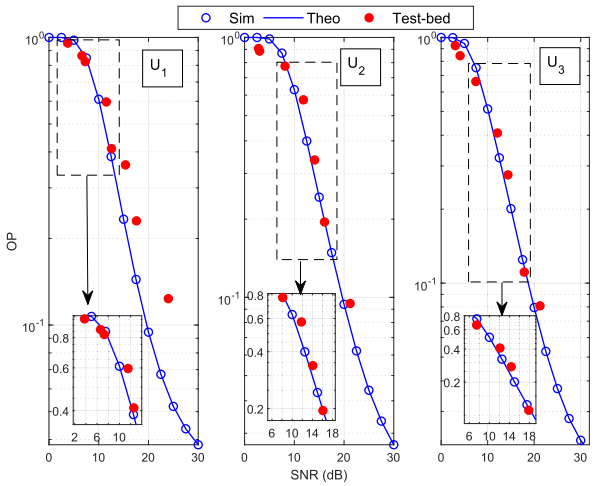

FIGURE 7. OP comparisons of test-bed implementation (USRP SDR) with simulation and theoretical results for MRT/MRC.

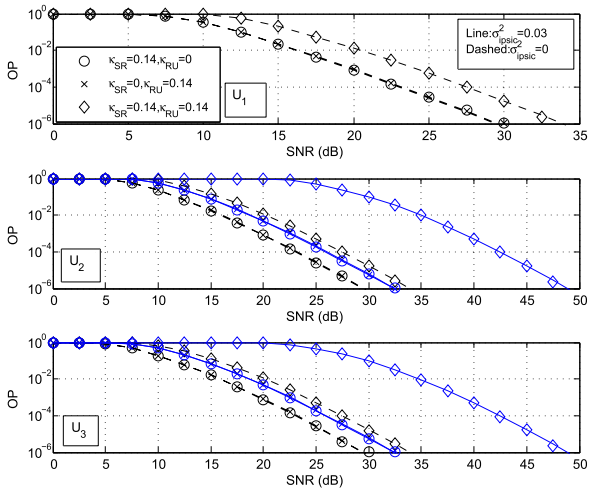

FIGURE 8. OP of users in case of different parameters of RHIs and ipSIC.

In Fig. 7, test-bed implementation results together with simulations are presented to support the analytical derivations for the hybrid scheme MRT/MRC. To obtain the OP curves, parameters provided in Sect. IV are used, that is ($N_S = 2; N_D = 2$), ($a_1 = 1/2; a_2 = 1/3; a_3 = 1/6$), ($d_{SR} = 0.5; d_1 = d_2 = d_3 = 0.5$), ($\gamma_{th,1} = 0.9; \gamma_{th,2} = 1.5; \gamma_{th,3} = 2$), $\sigma^2_{e,SR} = \sigma^2_{e,l} = 0.0388$, $\sigma^2_{ipsic} = 0.028$, ($\kappa_{SR} = 0.075$; $\kappa_{RU} = 0.075$), and $\mu = 0.3$. As seen in the figure, test-bed results (obtained by using USRP SDRs) can be observed to have been quite close to the simulation and analytical results, and exhibit the similar performance behavior. The difference between test and simulation results can be explained by cumulative estimation errors, unknown RHI parameters, and channel fading approximation. At the end of the experiment, it is expected that all users will have more or less similar OPs around 10^{-1}, by considering the continuation of outages in the high SNR region, as well as not reaching a precise error floor yet. It is worthy to note that test-bed results not only validate the theoretical analysis but also demonstrate feasibility of the investigated system in real-life manner. Although mobility (and Doppler spread) is absent in BS-R and $R - U_l$ links, dominant NLOS multipaths and HI introduce a non-negligible CFO. Our global reference signal distribution in Section IV-B improves the signal quality, increases SNR, and reduces synchronization complexity. The downlink NOMA demonstration shows that a global synchronization signal, such as global positioning systems (GPS), can significantly reduce computational complexity for NOMA users.

In Fig. 8, OP curves of all users are individually depicted for different RHIs and ipSIC parameters in case of $\mu = 0.2$, $\sigma^2_{e,SR} = \sigma^2_{e,l} = 0$, ($N_2 = 2; N_D = 2$), ($m_{SR} = 2; m_{LI} = 1; m_{RU} = 2$) configurations. It is obvious that the first user is not effected by ipSIC since it does not perform SIC cancellation. However, RHIs seriously deteriorate the performance of all users. In addition, ($\kappa_{SR} = 0.14; \kappa_{RU} = 0$) and ($\kappa_{SR} = 0; \kappa_{RU} = 0.14$) configurations exhibit the same OP performance,

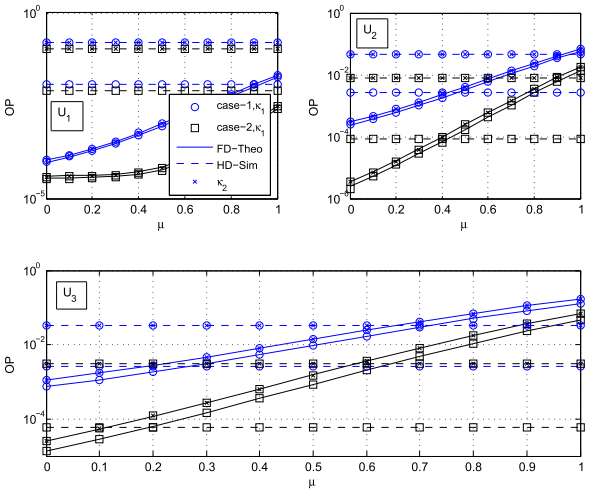

FIGURE 9. OP comparisons of the investigated FD-NOMA system with HD-NOMA versus μ for the fixed SNR = 15 dB.

thus RHIs in the first and second hops have the same effect on the system performance. From results of the second user, for an OP value of 10^{-4}, difference between $\sigma^2_{ipsic} = 0.03$ and $\sigma^2_{ipsic} = 0$ is approximately 15 dB in case of ($\kappa_{SR} = 0.14$; $\kappa_{RU} = 0.14$), while 3 dB in case of ($\kappa_{SR} = 0.14$; $\kappa_{RU} = 0$). Similar results can be obtained for the third user. This reveals that RHIs effect the performance more than ipSIC.

Fig. 9 represents OP comparisons of FD-NOMA (investigated) and HD-NOMA systems versus the quality of LI cancellation parameter μ in case fixed $SNR = 15$ dB, $\sigma^2_{e,SR} = \sigma^2_{e,l} = 0$, $\sigma^2_{ipsic} = 0$, $m_{SR} = m_{LI} = m_{RU} = 1$ and different RHIs parameters. In the figure, case-1:($N_S = 2; N_D = 2$), case-2:($N_S = 3; N_D = 2$), κ_1:($\kappa_{SR} = \kappa_{RU} = 0$) and κ_2:($\kappa_{SR} = \kappa_{RU} = 0.14$) definitions are made for simplicity. For fair comparison, threshold SIDNRs have the following relationship $\frac{1}{2}\log_2(1 + \gamma^{HD}_{th,l}) = \log_2(1 + \gamma^{FD}_{th,l})$. Also, we set threshold SIDNRs of HD-NOMA as $\gamma^{HD}_{th,1} = 0.9$, $\gamma^{HD}_{th,2} = 1.5$ and

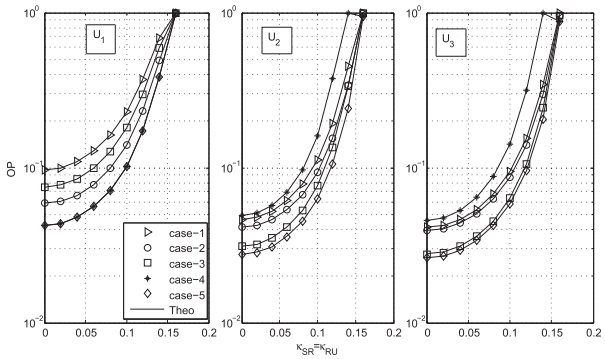

FIGURE 10. OP of users versus RHIs parameter in case of SNR = 15 dB.

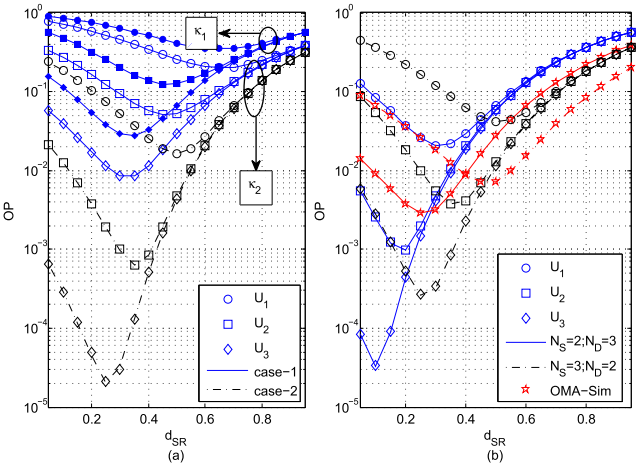

FIGURE 11. OP comparisons of the investigated FD-NOMA system with FD-OMA versus d_{SR} in case of $\mu = 0.2$, SNR = 15 dB, different fading and RHIs parameters, and number of antenna configurations.

$\gamma_{th,3}^{HD} = 2$ to ensure satisfying the condition of a_j-$\gamma_{th,j}(\xi_j + \tilde{\xi}_j + \vartheta_1) > 0$. As clearly seen from curves of the first user, FD-NOMA is better than HD-NOMA at the most of values μ, however performance gap between them decreases as the quality of LI cancellation gets worse. On the other hand, according to the second and third users, FD-NOMA outperforms HD-NOMA when the value of μ is below 0.49 and 0.26 for the configuration of (case-1,κ_1), respectively. Moreover, in the presence of RHIs (κ_2), FD-NOMA is better than HD-NOMA when $\mu \leq 0.9$ and $\mu \leq 0.65$ for the second and third users. Consequently, the quality of LI cancellation under RHIs can be worse than that of ideal HIs case for which FD-NOMA outperforms HD-NOMA.

Fig. 10 illustrates the OP performance of the investigated system versus RHIs parameters ($\kappa_{SR} = \kappa_{RU}$) for different effects of CEEs and ipSIC in case of fixed $SNR = 15$ dB, $N_S = N_D = 2$, $\mu = 0.2$ and $m_{SR} = m_{LI} = m_{RU} = 1$. For the figure to be better understandable, configurations are categorized into 5 cases as following case-1:($\sigma_{e,SR}^2 = 0.03$; $\sigma_{ipsic}^2 = 0$; $\sigma_{e,l}^2 = 0.03$), case-2:($\sigma_{e,SR}^2 = 0.03$; $\sigma_{ipsic}^2 = 0$; $\sigma_{e,l}^2 = 0$), case-3:($\sigma_{e,SR}^2 = 0$; $\sigma_{ipsic}^2 = 0$; $\sigma_{e,l}^2 = 0.03$), case-4:($\sigma_{e,SR}^2 = 0$; $\sigma_{ipsic}^2 = 0.03$; $\sigma_{e,l}^2 = 0$) and case-5:($\sigma_{e,SR}^2 = 0$; $\sigma_{ipsic}^2 = 0$; $\sigma_{e,l}^2 = 0$). As clearly seen from the results of all users, OP performances get worse as the effect of RHIs increase, even OPs equal to 1 under heavy RHIs effect. According to the first user, CEEs in the second hop worsen the performance more than that of in the first hop. However, in terms of the second and third users, CEEs in the first hop are much more effective than that of in the second hop. Moreover, ipSIC deteriorates the performance much more than CEEs in both hops for the second and third users.

Fig. 11 depicts OP performance of the investigated system versus distances between the BS and relay (d_{SR}) in case of fixed $SNR = 15$ dB and $\sigma_{e,SR}^2 = \sigma_{e,l}^2 = \sigma_{ipsic}^2 = 0$. The normalized distances in $R - U_l$ links are determined by $d_{RU_l} = 1 - d_{SR}$. In Fig. 11(a), κ_1:($\kappa_{SR} = \kappa_{RU} = 0.1$), κ_2:($\kappa_{SR} = \kappa_{RU} = 0$), case-1:($N_S = 2$;$N_D = 1$, $m_{SR} = m_{LI} = m_{RU} = 1$), case-2:($N_S = 2$;$N_D = 2$, $m_{SR} = 2$;$m_{LI} = 1$;$m_{RU} = 1$). Also, Fig. 11(b) is obtained for $\kappa_{SR} = \kappa_{RU} = 0.1$, $m_{SR} = m_{LI} = m_{RU} = 1$ and $\log_2(1 + \gamma_{th}^{OMA}) = \sum_{l=1}^{L} \log_2(1 + \gamma_{th,l})$ relation is used to obtain OMA curves. From Fig. 11(a), RHIs have the same level of effect on the performance at all values of distances for all users. It is observed that minimum OP is achieved when $d_{SR} < d_{RU_l}$ for the second and third users while $d_{SR} \geq d_{RU_l}$ for the first user since optimum relay location has a close relation with diversity order and array gain which are also provided in asymptotic analyses. On the other hand, from Fig. 11(b), FD-NOMA outperforms FD-OMA when the relay is close to the BS for the second and third users while FD-OMA is better at all values of d_{SR} for the first user.

VI. CONCLUSION

This paper analyzed the performance of MRT/MRC scheme in dual-hop NOMA FD AF relay networks over Nakagami-m fading channels by considering the effects of RHIs. In addition, CEEs and ipSIC were also taken into account in order for the system be more realistic. For performance criterion, exact OP for any user was derived together with tight lower bound and asymptotic expressions. Theoretical results validated by Monte Carlo simulations and USRP SDR-based implementations demonstrated that performance of the investigated FD-NOMA system is strictly limited by error floor in the high SNR region, even all users are exposed to the same level, if LI cancellation cannot be exploited. However, performance can be improved by increasing the number of antennas. On the other hand, all users can enjoy benefits of diversity order and array gain thanks to the quality of LI cancellation. Also, our analysis revealed that the MRT beamforming is better than MRC on the performance improvement of users with lower power allocations than user with the highest power allocation. However, under CEEs, performance trade-off between MRT and MRC schemes depends on imperfect channel conditions in both hops.

Besides CEEs and imperfect LI cancellation, RHIs seriously deteriorate the performance, such that it is much more effective for the second and third users relative to the first user, while it has no effect on diversity order. Under RHIs effect, LI cancellation process does not need to have a very high quality compared to ideal HIs case such that FD-NOMA outperforms HD-NOMA. It was also observed that imperfections which have the most and least deterioration effect on the performance are RHIs and CEEs, respectively. Furthermore, the minimum OP can be achieved with optimum relay location which has a close relation with diversity order and array gain, such that FD-NOMA outperforms FD-OMA when the relay is close to the BS for users with lower power allocations.

REFERENCES

[1] Y. Liu et al., "Evolution of NOMA toward next generation multiple access (NGMA) for 6G," *IEEE J. Sel. Areas Commun.*, vol. 40, no. 4, pp. 1037–1071, Apr. 2022.

[2] B. Makki, K. Chitti, A. Behravan, and M.-S. Alouini, "A survey of NOMA: Current status and open research challenges," *IEEE Open J. Commun. Soc.*, vol. 1, pp. 179–189, 2020.

[3] Y. Saito et al., "Non-orthogonal multiple access (NOMA) for cellular future radio access," in *Proc. IEEE Veh. Technol. Conf.*, Dresden, Germany, 2013, pp. 1–5.

[4] M. Aldababsa, M. Toka, S. Gokçeli, G. K. Kurt, and O. Kucur, "A tutorial on non-orthogonal multiple access for and beyond," *Wireless Commun. Mobile Comput.*, vol. 2018, pp. 1–24, 2018.

[5] Z. Ding, Z. Yang, P. Fan, and H. V. Poor, "On the performance of non-orthogonal multiple access in systems with randomly deployed users," *IEEE Signal Process. Lett.*, vol. 21, no. 12, pp. 1501–1505, Dec. 2014.

[6] S. Timotheou and I. Krikidis, "Fairness for non-orthogonal multiple access in systems," *IEEE Signal Process. Lett.*, vol. 22, no. 10, pp. 1647–1651, Oct. 2015.

[7] G. Gui, H. Sari, and E. Biglieri, "A new definition of fairness for non-orthogonal multiple access," *IEEE Commun. Lett.*, vol. 23, no. 7, pp. 1267–1271, Jul. 2019.

[8] Z. Ding, F. Adachi, and H. V. Poor, "The application of MIMO to non-orthogonal multiple access," *IEEE Trans. Wireless Commun.*, vol. 15, no. 1, pp. 537–552, Jan. 2016.

[9] M. Toka and O. Kucur, "Non-orthogonal multiple access with Alamouti space–time block coding," *IEEE Commun. Lett.*, vol. 22, no. 9, pp. 9697–9706, Sep. 2018.

[10] M. Toka and O. Kucur, "Performance analysis of OSTBC-NOMA system in the presence of practical impairments," *IEEE Trans. Veh. Technol.*, vol. 69, no. 9, pp. 9697–9706, Sep. 2020.

[11] M. Zeng, A. Yadav, O. A. Dobre, G. I. Tsiropoulos, and H. V. Poor, "Capacity comparison between MIMO-NOMA and MIMO-OMA with multiple users in a cluster," *IEEE J. Sel. Areas Commun.*, vol. 35, no. 10, pp. 2413–2424, Oct. 2017.

[12] Z. Ding, R. Schober, and H. V. Poor, "A general MIMO framework for NOMA downlink and uplink transmission based on signal alignment," *IEEE Trans. Wireless Commun.*, vol. 15, no. 6, pp. 4438–4454, Jun. 2016.

[13] F. Alavi, K. Cumanan, Z. Ding, and A. G. Burr, "Beamforming techniques for nonorthogonal multiple access in cellular networks," *IEEE Trans. Veh. Technol.*, vol. 67, no. 10, pp. 9474–9487, Oct. 2018.

[14] V. Ghanbarzadeh, M. Zahabi, H. Amiriara, F. Jafari, and G. Kaddoum, "Resource allocation in NOMA networks: Convex optimization and stacking ensemble machine learning," *IEEE Open J. Commun. Soc.*, vol. 5, pp. 5276–5288, 2024.

[15] G. Konstantopoulos and Y. Louët, "Deep learning aided beamforming for downlink non-orthogonal multiple access systems," *IEEE Open J. Commun. Soc.*, vol. 5, pp. 4337–4353, 2024.

[16] Z. Ding, M. Peng, and H. V. Poor, "Cooperative non-orthogonal multiple access in systems," *IEEE Commun. Lett.*, vol. 19, no. 8, pp. 1462–1465, Aug. 2015.

[17] J.-B. Kim and I.-H. Lee, "Non-orthogonal multiple access in coordinated direct and relay transmission," *IEEE Commun. Lett.*, vol. 19, no. 11, pp. 2037–2040, Nov. 2015.

[18] J. Men, J. Ge, and C. Zhang, "Performance analysis for downlink relaying aided non-orthogonal multiple access networks with imperfect CSI over Nakagami-*m* fading," *IEEE Access*, vol. 5, pp. 998–1004, 2017.

[19] Y. Zhang, J. Ge, and E. Serpedin, "Performance analysis of non-orthogonal multiple access for downlink networks with antenna selection over Nakagami-*m* fading channels," *IEEE Trans. Veh. Technol.*, vol. 66, no. 11, pp. 10590–10594, Nov. 2017.

[20] X. Yan, J. Ge, Y. Zhang, and L. Gou, "NOMA-based multiple-antenna and multiple-relay networks over Nakagami-m fading channels with imperfect CSI and SIC error," *IET Commun.*, vol. 12, no. 17, pp. 2087–2098, 2018.

[21] M. Aldababsa and O. Kucur, "Performance of cooperative multiple-input multiple-output NOMA in Nakagami-m fading channels with channel estimation errors," *IET Commun.*, vol. 14, no. 2, pp. 274–281, 2020.

[22] M. Duarte, C. Dick, and A. Sabharwal, "Experiment-driven characterization of full-duplex wireless systems," *IEEE Trans. Wireless Commun.*, vol. 11, no. 12, pp. 4296–4307, Dec. 2012.

[23] C. Zhong and Z. Zhang, "Non-orthogonal multiple access with cooperative full-duplex relaying," *IEEE Commun. Lett.*, vol. 20, no. 12, pp. 2478–2481, Dec. 2016.

[24] T. M. C. Chu and H.-J. Zepernick, "Performance of non-orthogonal multiple access system with full-duplex relaying," *IEEE Commun. Lett.*, vol. 22, no. 10, pp. 2084–2087, Oct. 2018.

[25] M. Mohammadi et al., "Beamforming design and power allocation for full-duplex non-orthogonal multiple access cognitive relaying," *IEEE Trans. Commun.*, vol. 66, no. 12, pp. 5952–5965, Dec. 2018.

[26] V. Özduran, N. Nomikos, E. Soleimani-Nasab, I. S. Ansari, and P. Trakadas, "Relay-aided uplink NOMA under non-orthogonal CCI and imperfect SIC in networks," *IEEE Open J. Veh. Technol.*, vol. 5, pp. 658–680, 2024.

[27] T. Schenk, *RF Imperfections in High-Rate Wireless Systems: Impact and Digital Compensation*, 1st ed. Dordrecht, The Nederlands: Springer, 2008.

[28] E. Björnson, M. Matthaiou, and M. Debbah, "A new look at dual-hop relaying: Performance limits and hardware impairments," *IEEE Trans. Commun.*, vol. 61, no. 11, pp. 4512–4525, Nov. 2013.

[29] E. Björnson, J. Hoydis, M. Kountouris, and M. Debbah, "Massive MIMO systems with non-ideal hardware: Energy efficiency, estimation, and capacity limits," *IEEE Trans. Inf. Theory*, vol. 60, no. 11, pp. 7112–7139, Nov. 2014.

[30] X. Li et al., "Security analysis of multi-antenna NOMA networks under I/Q imbalance," *Electronics*, vol. 8, no. 1327, pp. 1–17, 2019.

[31] M. Toka and O. Kucur, "Performance of MRT/RAS MIMO-NOMA with residual hardware impairments," *IEEE Wireless Commun. Lett.*, vol. 10, no. 5, pp. 1071–1074, May 2021.

[32] F. Ding, H. Wang, S. Zhang, and M. Dai, "Impact of residual hardware impairments on non-orthogonal multiple access based amplify-and-forward relaying networks," *IEEE Access*, vol. 6, pp. 15117–15131, 2018.

[33] X. Li et al., "Residual transceiver hardware impairments on cooperative NOMA networks," *IEEE Trans. Wireless Commun.*, vol. 19, no. 1, pp. 680–695, Jan. 2020.

[34] C. B. Le, D. T. Do, and M. Voznak, "Exploiting impact of hardware impairments in NOMA: Adaptive transmission mode in FD/HD and application in Internet-of-Things," *Sensors*, vol. 19, no. 1293, pp. 1–24, 2019.

[35] C. Deng, M. Liu, X. Li, and Y. Liu, "Hardware impairments aware full-duplex NOMA networks over Rician fading channels," *IEEE Syst. J.*, vol. 15, no. 2, pp. 2515–2518, Jun. 2021.

[36] C. K. Singh, P. K. Upadhyay, and J. J. Lehtomäki, "Performance analysis and deep learning assessment of full-duplex overlay cognitive radio NOMA networks under non-ideal system imperfections," *IEEE Trans. Cogn. Commun. Netw.*, vol. 9, no. 3, pp. 664–682, Jun. 2023.

[37] T. Lo, "Maximum ratio transmission," *IEEE Trans. Commun.*, vol. 47, no. 10, pp. 1458–1461, Oct. 1999.

[38] M. K. Simon and M. S. Alouini, *Digital Communications Over Fading Channels*, 2nd ed. Hoboken, NJ, USA: Wiley, 2005, vol. 95.

[39] M. Medard, "The effect upon channel capacity in wireless communications of perfect and imperfect knowledge of the channel," *IEEE Trans. Inf. Theory*, vol. 46, no. 3, pp. 933–946, May 2000.

[40] B. C. Nguyen et al., "Impact of hardware impairments on the outage probability and ergodic capacity of one-way and two-way full-duplex relaying systems," *IEEE Trans. Veh. Technol.*, vol. 69, no. 8, pp. 8555–8567, Aug. 2020.
[41] A. Hasan and J. Andrews, "Cancellation error statistics in a power-controlled CDMA system using successive interference cancellation," in *Proc. IEEE Int. Symp. Spread Spect. Techn. App.*, Sydney, NSW, Australia, 2004, pp. 1–5.
[42] D. Tweed, M. Derakhshani, S. Parsaeefard, and T. Le-Ngoc, "Outage-constrained resource allocation in uplink NOMA for critical applications," *IEEE Access*, vol. 5, pp. 27636–27648, 2017.
[43] I. S. Gradshteyn and I. M. Ryzhic, *Table of Integrals, Series, and Products*, 6th ed. New York, NY, USA: Academic Press, 2000.
[44] H. David and H. Nagaraja, *Order Statistics*, 3rd ed. Hoboken, New Jersey, USA: Wiley, 2003.
[45] Z. Wang and G. B. Giannakis, "A simple and general parameterization quantifying performance in fading channels," *IEEE Trans. Commun.*, vol. 51, no. 8, pp. 1389–1398, Aug. 2003.
[46] K. B. Oldham, J. Myland, and J. Spanier, *An Atlas of Functions With Equator the Atlas Function Calculator*, 2nd ed. New York, NY, USA: Springer, 2008.
[47] M. A. Durmaz et al., "A four-user non-orthogonal multiple access system implementation in software defined radios," in *Proc. IEEE Int. Black Sea Conf. Commun. Netw.*, Odessa, Ukraine, 2020, pp. 1–5.
[48] H. A. Mahmoud and H. Arslan, "Error vector magnitude to SNR conversion for nondata-aided receivers," *IEEE Trans. Wireless Commun.*, vol. 8, no. 5, pp. 2694–2704, May 2009.
[49] D. Pauluzzi and N. Beaulieu, "A comparison of SNR estimation techniques for the AWGN channel," *IEEE Trans. Commun.*, vol. 48, no. 10, pp. 1681–1691, Oct. 2000.
[50] A. Hussain, A. Alayon Glazunov, B. Einarsson, and P.-S. Kildal, "Antenna measurements in reverberation chamber using USRP," *IEEE Trans. Antennas Propag.*, vol. 64, no. 3, pp. 1152–1157, Mar. 2016.
[51] Z. Ding, R. Schober, and H. V. Poor, "Unveiling the importance of SIC in NOMA systems—Part 1: State of the art and recent findings," *IEEE Commun. Lett.*, vol. 24, no. 11, pp. 2373–2377, Nov. 2020.

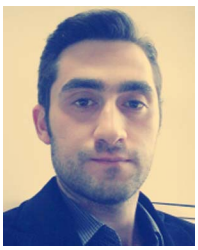

MESUT TOKA (Member, IEEE) received the Ph.D. degree in electronics engineering from Gebze Technical University (GTU), Gebze/Kocaeli, Türkiye, in 2021. He was a Postdoctoral Researcher in electrical and computer engineering with Ajou University, Suwon, South Korea. He was also a Research and Teaching Assistant with GTU, where he is currently an Assistant Professor of electronics engineering. His research interests include cooperative communications, full-duplex communications, multiple access techniques, reconfigurable intelligent surfaces, and space-air-ground integrated networks.

ERAY GÜVEN (Graduate Student Member, IEEE) received the B.S. degree in electronics and communication engineering from Istanbul Technical University, Istanbul, Türkiye in 2021. He is currently working toward the Ph.D. degree in electrical engineering with Polytechnique Montréal, Montréal, QC, Canada.

GÜNEŞ KARABULUT KURT (Senior Member, IEEE) received the B.S. degree (with Hons.) in electronics and electrical engineering from Boğaziçi University, Istanbul, Türkiye, in 2000, and the M.A.Sc. and Ph.D. degrees in electrical engineering from the University of Ottawa, ON, Canada, in 2002 and 2006, respectively. From 2000 to 2005, she was a Research Assistant with CASP Group, University of Ottawa. From 2005 to 2006, she was with TenXc Wireless, Canada. From 2006 to 2008, she was with Edgewater Computer Systems Inc., Canada. From 2008 to 2010, she was with Turkcell Research and Development Applied Research and Technology, Istanbul. From 2010 to 2021, she was with Istanbul Technical University. She is currently a Full Professor of electrical engineering with Polytechnique Montréal, Montréal, QC, Canada. She is also an Adjunct Research Professor with Carleton University, Ottawa, ON, Canada. She was the recipient of the Turkish Academy of Sciences Outstanding Young Scientist (TÜBA-GEBIP) Award in 2019. She is also a member for the IEEE WCNC Steering Board and an Associate Technical Editor (ATE) of *IEEE Communications Magazine*. She is also a Marie Curie Fellow.

OĞUZ KUCUR (Member, IEEE) received the B.S. degree in electronics and telecommunication engineering from Istanbul Technical University, Istanbul, Türkey, in 1988, and the M.S. and Ph.D. degrees in electrical and computer engineering from the Illinois Institute of Technology (IIT), Chicago, IL, USA, in 1992 and 1998, respectively. From 1996 to 1998, he was a Teaching Assistant with IIT. From 1998 to 1999, he was an Assistant Professor with the Department of Electrical Engineering, South Dakota State University, Brookings, SD, USA. Since 1999, he has been with the Department of Electronics Engineering, Gebze Technical University, Türkey, where he is currently a Professor. His research interests include fading channels and diversity techniques, multi-user communications, MIMO, and cooperative communications.